IEEE Access
Multidisciplinary | Rapid Review | Open Access Journal

Received July 27, 2020, accepted August 1, 2020, date of publication August 5, 2020, date of current version August 17, 2020.

Digital Object Identifier 10.1109/ACCESS.2020.3014285

A Novel Method and Exoskeletons for Whole-Arm Gravity Compensation

JOSHUA HULL*, RANGER TURNER*, ATHULYA A. SIMON, AND ALAN T. ASBECK
Mechanical Engineering Department, Virginia Tech, Blacksburg, VA 24061, USA

Corresponding author: Alan T. Asbeck (aasbeck@vt.edu)

*Joshua Hull and Ranger Turner contributed equally to this work.

This project was funded by the Mechanical Engineering Department at Virginia Tech and the Virginia Tech Open Access Subvention Fund, and Joshua Hull was also supported by a Science, Mathematics, and Research for Transformation (SMART) fellowship.

ABSTRACT We present a new method for providing gravity compensation to a human or robot arm. This method allows the arm to be supported in any orientation, and also allows for the support of a load held in the hand. We accomplish this with a pantograph, whereby one portion of the linkage duplicates the arm's geometry, and another portion of the linkage contains a scaled copy of the arm. Forces applied to the scaled copy are transferred back to the original arm. We implement these concepts with two exoskeletons: the Panto-Arm Exo, a low-profile exoskeleton that supports the arm's weight, and the Panto-Tool Exo that supports a mass held in the hand. We present two linkages used for pantographs, and analyze how different linkage dimensions and their positioning relative to the body affect the forces providing gravity compensation. We also measured the effect of the Panto-Arm exoskeleton on fourteen subjects' arm muscles during static holding tasks and a task in which subjects drew horizontal and vertical lines on a whiteboard. Even though the Panto-Arm Exo linkage geometry and forces were not optimized, it reduced the Mid Deltoid by 33-43% and the Biceps Brachii by up to 52% in several arm postures.

INDEX TERMS Exoskeleton, gravity compensation, arm support, pantograph, electromyography.

I. INTRODUCTION

Arm-support devices that provide gravity compensation to a human or load held in the hand have existed for more than 20 years. These generally have two primary fields of use: in industrial settings, where workers must hold tools or their hands in the air for extended periods of time, and in medical settings, where individuals who lack arm strength are assisted in raising their arms.

For industrial applications, there are two main types of devices. The first type includes exoskeletons that solely help workers raise their hands, and any tools they are holding, for overhead work. Some notable examples of these include the Ekso Bionics EksoVest [1], SuitX ShoulderX [2], Ottobock Paexo [3], [4], and Levitate AIRFRAME [5]. These all have a support under the upper arm, pushing up under the tricep, and thus do not effectively support the forearm or tool if the arm is in other postures.

The second type includes gravity compensation devices that support a heavy (10+ kg) tool or load. Some examples include the EXHAUSS Stronger exoskeleton [6], an exoskeleton from the Robomate project [7], [8], and the Lockheed FORTIS [9], [10]. These devices can alternatively be mounted to a railing or other grounded surface (e.g. the Ekso Bionics EksoZeroG [11]) instead of worn as an exoskeleton. Nearly all of them use a parallelogram-based gravity compensation scheme where a spring on a diagonal allows one end of a parallelogram to support a constant force, even as the two ends move vertically with respect to one another [12].

In the medical field, there are a number of mechanisms used to passively support the weight of a person's arm; an excellent overview is in [13]. These are almost always mounted to a table or wheelchair. Some notable examples include the Wilmington Robotic Exoskeleton (WREX) [14], which supports the upper arm and forearm separately with parallelogram linkages and elastic bands; SaeboMAS [15], which uses a single parallelogram linkage; A-gear [16], which supports the whole arm with two elastic bands and a novel linkage; Armon [17], [18], which uses a novel linkage and several extension springs; Armeo Spring [19], a device for rehabilitation; Freebal [20], which supports the arm with cables from a gantry; and LIGHTarm [21], which also includes a powered version.

The associate editor coordinating the review of this manuscript and approving it for publication was Agustin Leobardo Herrera-May.

FIGURE 1. (a), Picture of the Panto-Arm Exo, an arm support exoskeleton, showing its construction. (b), Picture of the Panto-Arm Exo, showing the upper range of motion in the current version. (c), Pictures of the Panto-Arm Exo worn under a shirt. (d), Panto-Tool Exoskeleton designed to support a load at the user's hand.

There have also been a number of devices developed to passively support the weight of a robot's arm. These can be very beneficial toward making a robot more human-safe, as the arm's mass can be supported by an un-powered spring-based system, enabling smaller motors to be used at the robot's joints. Some examples of systems to support a robot arm, as well as other mechanisms that provide passive gravity compensation not specifically for a robot, are in [22]–[32].

For both rehabilitation and industrial applications, a number of powered exoskeletons have also been developed, including many with gravity compensation [33]–[35]. There has also been much work on gravity compensation algorithms that can be applied to both powered exoskeletons and robot arms [36]–[40], with a recent review in [41]. Active gravity compensation schemes are effective in that they can support the weight of a human's arm or a load they pick up automatically, without adjustments from the user. However, the addition of motors, sensors, and electronics leads to a system that is potentially much more complicated and heavier than a passive spring-based one.

Despite this extensive prior work, current passive arm- and tool-support gravity compensation devices have several shortcomings. Exoskeletons for overhead industrial work are limited in their usefulness to situations where the worker's arms are nearly directly over their head. If the worker extends their hands forward, or rotates their shoulder, then their forearm and shoulder are no longer appropriately supported. The exoskeletons that support tools are relatively large and bulky, and may interfere with other objects in the worker's environment. The existing medical arm support devices almost entirely consist of table- or wheelchair-mounted products, preventing their use in many activities of daily living. Most parallelogram-based devices tend to be bulky, as the parallelograms must lie in a vertical plane, thereby not aligning with the user's elbow in most arm configurations.

We have created a novel concept for gravity compensation that addresses many of the shortcomings in prior devices [42]. It can be made into an exoskeleton that is both light-weight (1.6 kg) and low-profile enough to be worn under a loose-fitting shirt or jacket (Fig. 1(a)-(c)). The concept uses a linkage that supports the entire arm using a single spring or force-producing element and changes the shoulder torque automatically as the forearm moves closer to or away from the body. Other variants of the device can support a tool or load in the wearer's hand instead of or in addition to the weight of the arm (Fig. 1(d)). In each of these cases, the linkage closely follows the kinematics of the arm, making it suitable for an exoskeleton. The same concepts could be used to provide gravity compensation for a humanoid robot arm instead of a human arm, in combination with small motors to control each joint.

In the rest of this article, we first provide an overview of our exoskeletons and their means of operation. We then analyze the effects on the gravity compensation forces of changing several linkage parameters and varying the offset between the linkage and the body. We present the results of mechanical experiments on one of our exoskeletons, and human subject testing results on muscle activation changes due to the exoskeleton.

II. OVERVIEW AND CONCEPT

A. OVERVIEW

Our concept makes use of a single upward force on the forearm in conjunction with the shoulder to support the arm's weight, similar to the derivation by Herder *et al.* [43] and used by a number of devices such as the SaeboMAS [15] and Armon [17] arm supports. We provide a brief explanation following the diagram in Fig. 2(a). The center of mass of the entire arm ($m_{wholearm}$) is on the line connecting the centers of mass for the upper arm ($m_{upperarm}$) and forearm ($m_{forearm}$). If a line, here referred to as the "Arm balancing line," is drawn from the shoulder through the whole arm center of mass, it intersects the forearm at the "arm support point," which lies fairly close to the elbow. If the appropriate upward force is provided to the arm at the arm support point, then the arm will be perfectly supported by the shoulder and that force.

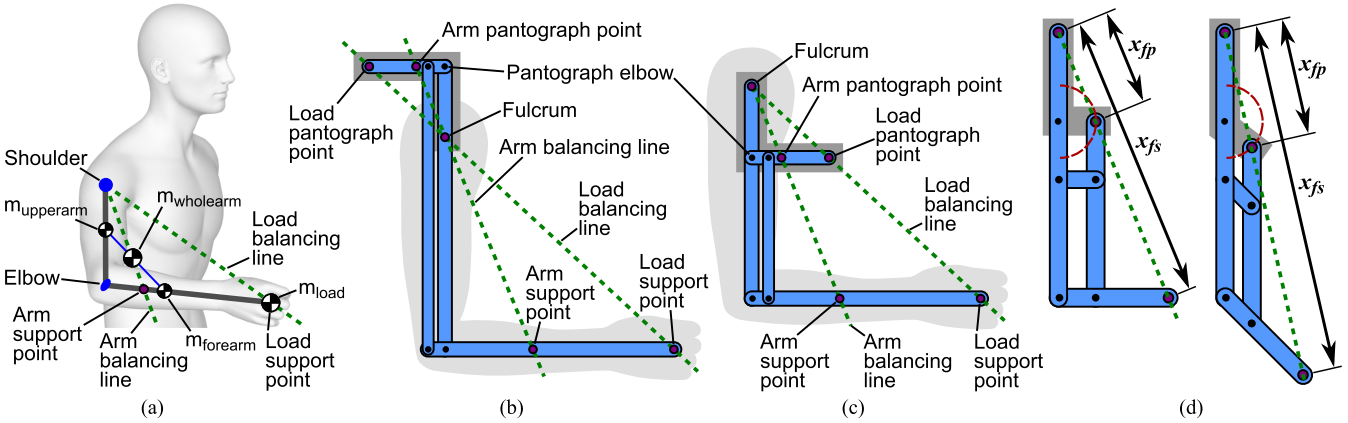

FIGURE 2. (a), Variables showing how the arm can be fully supported by the shoulder and a single balancing point located on the forearm. (b), Geometry of a Class 1 pantograph implemented with a four bar linkage. (c), Geometry of a Class 3 pantograph implemented with a four bar linkage. (d), Illustration of how the pantograph point and arm support point maintain the same ratio of distances as the elbow moves. The drawing also shows a virtual forearm segment: the load pantograph point follows the red dashed line as the elbow angle changes. In (b) and (c), the biological arm is shown by a shaded light gray region; in (b)-(d), the pantograph arm is shown by a darker gray region.

Note that this holds true regardless of the arm's elevation (shoulder flexion or abduction) and the rotation of the arm around the arm balancing line. In this analysis, the shoulder is assumed to be a spherical joint.

We extend this reasoning to a mass held in the hand, such as a box or tool. In this case, we assume the mass is a point mass (m_{load}), and so the "load support point" is at the hand and the "load balancing line" intersects the hand. As with the arm, if an appropriate upward force is provided at the load support point, the mass will be balanced independent of its rotation around the load balancing line. In general, we would like to provide gravity compensation both to the arm (and any mass distributed along it, such as the exoskeleton itself or other protective apparel) as well as a load in the hand.

B. PANTOGRAPHS

To achieve the behavior of an upward force at the arm support point and/or the load support point independent of the arm's configuration, we use a three-dimensional pantograph mechanism. Pantographs have been used since the 1600s as a means of making a copy of a letter while writing it [44], and some groups have used pantographs for gravity compensation in conjunction with masses [45] or with springs for each of the upper arm and forearm [46]. In general, a pantograph will duplicate the motion of one part of a linkage with a second part of the linkage. It is possible for one part of the linkage to be scaled with respect to the other part, thereby creating a transmission ratio between the two copies. In our case, we use pantographs to create a scaled copy of the biological arm. One part of the linkage is aligned with the arm, and the second part duplicates the arm's geometry and motion but on a smaller scale. We then apply forces to the scaled copy, and the pantograph linkage transmits these forces back to the arm to provide gravity compensation. Detailed diagrams can be seen in Fig. 2(b)-(d). In our implementation, we have used a parallel four-bar linkage to create the pantographs, although other methods are possible, for example creating two copies of an arm connected by pulleys and cables [42].

One possible instantiation of this concept is when the pantograph is configured as a Class 1 lever (Fig. 2(b)), which we refer to as a Class 1 pantograph. There is a fulcrum, which acts as both the biological shoulder and shoulder of the scaled copy, which we call the "pantograph shoulder." To achieve three-dimensional motion, the fulcrum is a spherical joint or equivalent combination of single-axis rotational joints. One side of the linkage matches the biological arm, and includes the arm support point and load support point. On the far side of the fulcrum is the pantograph copy of the arm, which we refer to as the "pantograph arm." In the Class 1 pantograph, the pantograph arm is rotated 180° from the biological arm. It has a portion corresponding to the upper arm, between the fulcrum and the "pantograph elbow," and a portion corresponding to the forearm, beyond the pantograph elbow. On the pantograph forearm there is an arm pantograph point that falls on the arm balancing line and there is a load pantograph point that falls on the load balancing line. In the Class 1 pantograph, there is an upward force on the fulcrum, and downward forces on both the arm/load support points and the arm/load pantograph points. Note that with this linkage, when the biological arm moves downward, the pantograph arm moves upward, and thus is mirrored.

The pantograph can be also be configured as a Class 3 lever (Fig. 2(c)). This topology is very similar to that of the Class 1 pantograph, except the pantograph arm maintains the same orientation as the biological arm. The fulcrum is on one end, and experiences a downward force, while the arm pantograph point and load pantograph point both experience upward forces.

With both of the Class 1 and Class 3 linkages, forces can be provided to either or both the arm pantograph point and load pantograph point. Also note that we have arbitrarily called the "fulcrum" as the point which is constrained from moving vertically, while the arm and load pantograph points move up

and down to accommodate the motion of the arm. In practice, it is possible to make constructions where both the fulcrum and pantograph points can translate vertically, for example if constant force springs were attached to each of them. Also note that while planar four-bar linkages are illustrated in these diagrams, the arm support point and load support point are located in the center of the arm and load, respectively. Thus, depending on how the exoskeleton is constructed, there may be an offset between the support points on the linkage and true support points.

The behavior of the pantograph linkage as the elbow moves is illustrated in Fig. 2(d) for a Class 3 system. There, it can be seen that the distance from the fulcrum to the arm pantograph point is x_{fp}, and the distance from the fulcrum to the arm support point is x_{fs}. With the pantograph linkage, the ratio between these points remains constant. We define this ratio as the pantograph ratio R:

$$R = x_{fs}/x_{fp} \ . \tag{1}$$

Since this ratio remains constant, a constant upward force on the arm support point or load support point can be achieved by placing a constant downward force at the arm pantograph point or load pantograph point, respectively. With a Class 1 pantograph, for example, if the downward force at a support point is $F_{support}$ and the downward force at the pantograph point is F_{panto}, to have balanced moments M about the fulcrum we must have:

$$\Sigma M = 0: \quad F_{support}\, x_{fs} = F_{panto}\, x_{fp} \tag{2}$$

$$\Rightarrow F_{panto} = (x_{fs}/x_{fp})\, F_{support} = R\, F_{support} \tag{3}$$

Thus, the forces in the vertical direction (at the pantograph points, fulcrum, and support points) are always constant and the linkage remains balanced regardless of how it moves. Only one downward force is required to balance the arm's mass, and a second downward force can be used to support the mass of a tool. It may be beneficial to use only one of these points, for example if only the arm is to be supported, or if an industrial exoskeleton supports only a tool but not the wearer's arm. The points can also be used in combination: a constant force at the arm pantograph point can support the weight of the arm and the exoskeleton, while a variable force at the load pantograph point could support a load that is picked up and put down.

C. MECHANICAL DESIGNS

We have constructed two prototype exoskeletons to demonstrate the concept of gravity compensation using a pantograph. These are shown in Fig. 1.

1) CLASS 3 PANTOGRAPH EXOSKELETON

We created an exoskeleton based on a Class 3 pantograph to support the arm's weight. We call this the "Panto-Arm Exo," which is short for Pantograph Arm Support Exoskeleton, and it is shown in Fig. 1(a)-(c) and Fig. 3. The exoskeleton is

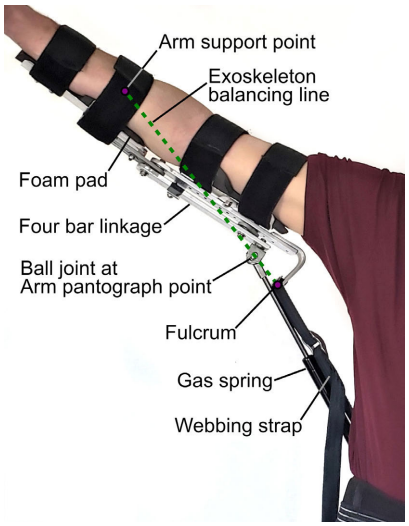

FIGURE 3. Details of the mechanical design of the Panto-Arm Exo, which has a Class 3 pantograph.

based around a four bar linkage with the topology shown in Fig. 2(d). This linkage uses a "virtual" bar to act as the forearm segment of the pantograph, in that there is no link directly connecting the pantograph elbow to the arm pantograph point; instead, a point on the link parallel to the upper arm follows the correct trajectory of the arm pantograph point. The motion of this point is shown by the red dashed line. For comparison, in Fig. 2(c) a mechanical link rotates around the pantograph elbow. There are several benefits of the construction in Fig. 2(d) with the virtual bar. First, the four bar linkage can be composed of links stacked in the pattern shown in Fig. 2(d), which leads to the linkage being able to rotate a full 180° and the arm pantograph point being located on the bottom of the stack of four bar links. Thus, there is a full range of motion and the force-producing element beneath the linkage is unobstructed. It is also possible to achieve a full range of motion with other stacking orders of the links, but the mechanism geometries are slightly more complicated. Second, the arm pantograph point may be relatively close to the pantograph elbow. Placing the arm pantograph point as in Fig. 2(d) provides additional space for bearings to be mounted to the two links. Finally, with this construction, the arm pantograph point does not rotate as the forearm moves, but instead translates through an arc while keeping its orientation. This may make it easier to create a joint that connects it to a force-producing element underneath it. The down side of this construction is that only the arm pantograph point or load pantograph point, but not both, can be included in the linkage without excessive complexity.

In our exoskeleton, the four bar linkage was made of 6 mm thick aluminum bars, and the pivots were made with ball bearings. It has a pantograph ratio of 6, with a distance of 24 cm between the fulcrum and arm support point and a distance of 4 cm between the fulcrum and arm pantograph point when the arm is fully outstretched. Attached to the four bar linkage are arm cuffs to connect to the user's arm.

These are positioned both above and below the elbow, and were made as long as reasonable (20.2 cm in the direction parallel to the arm) to keep the exoskeleton linkage aligned with the arm. The use of an arm cuff on each side of the elbow helps keep the elbow aligned with the pivot on the linkage. To create an upward force on the arm pantograph point, we use a gas spring with a strength depending on the wearer's weight (SUSPA Model #s C16-14873 or C16-14874, with initial forces of 88.9 N or 133.4 N and maximum forces of 112.6 N or 169.0 N, respectively). A gas spring was chosen because it can have a large travel with a force that is approximately constant (typically varies by $<30\%$) and it has a package convenient for mounting. Between the gas spring and the four bar linkage there is a joint composed of a revolute joint attached to the linkage followed by a ball joint connected to the gas spring. The gas spring's axial rotation also acts as a roll degree of freedom. On its lower side, the gas spring is connected to a 23.3 cm wide $\times$ 12.2 cm tall $\times$ 1 mm thick plate mounted to an elastic waist belt. The plate is backed by 1 cm thick foam to provide cushioning for the wearer. To create a downward force on the fulcrum, a webbing strap with a buckle connects the fulcrum to the plate on the waist belt. The webbing is flexible in all directions, making the location where it connects to the fulcrum act as a spherical joint. Additionally, its connection to the metal at the fulcrum permits rotation through the use of a grommet in the webbing. The buckle allows the entire exoskeleton to be adjusted in height for different size wearers simply by lengthening or shortening the webbing; the gas spring will expand or contract to be the correct length.

A bent piece of metal is connected to the end of the planar four bar linkage, curving down 5.4 cm to where the webbing strap was attached at the fulcrum. This was so that the fulcrum would occur on the line passing through the center of the arm (i.e., several centimeters above the planar four bar linkage) and through the pantograph point on the exoskeleton, which is collocated with the joint between the gas spring and four bar linkage. This line is labeled the ''exoskeleton balancing line'' in Fig. 3, as it is angled with respect to the arm and thus does not coincide with the biological arm balancing line. Even though the exoskeleton balancing line is not coincident with the arm balancing line, the pantograph geometry still acts to duplicate the motion of the arm and create an upward force at the arm support point.

2) CLASS 1 PANTOGRAPH EXOSKELETON

Our Class 1 pantograph exoskeleton, the ''Panto-Tool Exo'' (short for Pantograph Tool Support Exoskeleton), is shown in Fig. 1(d). It is designed to support heavy loads at the hand, but does not support the arm or exoskeleton structure. The exoskeleton consists of a waist belt, frame plate on the wearer's back, and shoulder straps to secure the exoskeleton to the back. The exoskeleton fulcrum is connected to the frame plate with three single-axis rotational joints: a joint with a vertical axis on the frame plate, a joint with an axis pointing toward the wearer's torso parallel to the ground, and a joint parallel to the upper arm. Together, the three joints act as a roll-pitch-roll joint and provide three degrees of freedom at the shoulder. The fulcrum's location is several centimeters behind the wearer's shoulder. The four bar linkage extends along the wearer's arm but is not attached to the arm; a handle near the end allows them to grasp it.

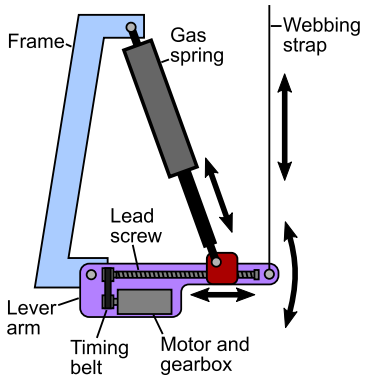

FIGURE 4. Diagram of the mechanism providing force for the Panto-Tool Exo, a Class 1 pantograph.

A downward force at the back is provided by a gas spring and lever arm, illustrated in Fig. 4. The mechanism includes a lead screw and motor, so the lower end of the gas spring can be moved along the lever arm, changing the force. When the gas spring is moved very close to the pivot between the frame plate and lever arm, the gas spring has a very small moment arm and creates zero force. For heavy loads, the gas spring can be moved closer to the end of the lever arm. The end of the lever arm is connected to the load pantograph point on the exoskeleton with a piece of webbing.

With a gas spring that has an initial force of 900 N and a maximum force of 1200 N (Kaller Model # R19-100 Yellow), the exoskeleton is able to support a mass of 10 kg at the hand. The exoskeleton uses a pantograph ratio of 6, with a distance from the hand to the fulcrum of 70.4 cm and a distance from the fulcrum to the load pantograph point of 11.7 cm when the arm is fully outstretched.

III. ANALYSIS

We performed analysis of both the Class 1 and Class 3 pantograph topologies, determining the forces on the arm support point or tool support point as the wearer adopted several poses and as they moved their shoulder or elbow. This analysis was repeated as several mechanical parameters of the exoskeletons were adjusted, showing the trends in force production and sensitivity of the results to the exoskeletons' geometry. We additionally calculated the locations of the arm support point for different sized humans.

A. ARM SUPPORT EXOSKELETON ANALYSIS

1) ARM LENGTH AND CENTER OF MASS SENSITIVITY

The optimal exoskeleton would support the user's arm directly at the arm support point. Different people will have different arm support points, and determining the arm

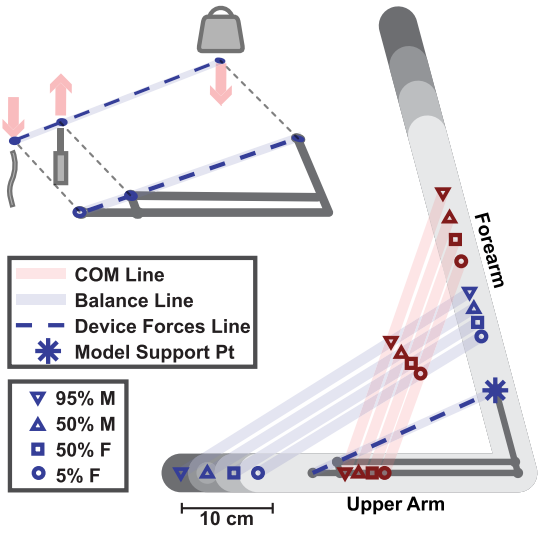

FIGURE 5. Representation of the exoskeleton for the Transverse Plane Elbow Sweep. The upper arm and forearm lengths for the 95th and 50th percentile Male and 50th and 5th percentile Female are shown as thick gray lines, aligned at the elbow. These percentiles show the full range of human arm sizes. The centers of mass (COM) of the forearm and upper arm are plotted on the thick gray lines with different symbols as indicated in the figure legend. They are connected by a red line, on which lies the whole-arm center of mass. The arm balancing line is shown with a blue line that extends from the shoulder (symbol at the far left of the upper arm segment) through the whole-arm center of mass and to the forearm. The intersection of the arm balancing line with the forearm is indicated by another symbol. The arm lengths are taken from [47], and the center of mass locations and arm balance lines are calculated using values from [47], [48]. The geometry of our Panto-Arm exoskeleton is also drawn on the diagram, with thin gray lines, an asterisk indicating where it pushes up on the forearm (Model Support Pt.), and a blue dashed line indicating its balancing line.

support point requires knowing the center of mass of the arm, which is not easily measurable on live subjects [48]. To gain understanding of the range of arm sizes and locations of the arm support point on different individuals, we plotted the arm lengths and the centers of mass of the arms for the 5th, 50th, and 95th percentiles in both males and females ([47], [48]) in Fig. 5. In the figure, the upper arm and forearm links are shown with the thick gray lines, with different shades of gray for different sizes of person; the 5th percentile female has the shortest set of lines, and the 95th percentile male has the longest set of lines. These are shown aligned at the elbow. For each size individual, the center of mass of the forearm is shown with a red symbol on the forearm link, and the center of mass of the upper arm is shown with a red symbol on the upper arm link. These centers of mass are connected with a light red line (“COM Line”), and the center of mass of the entire arm is shown near the center of this line. A blue symbol is drawn at the shoulder for each individual, and a blue line extends from the shoulder through the whole-arm center of mass. This blue line is the arm balancing line, and the location where it intersects the forearm (marked with a blue symbol) is the arm support point.

Shown in Fig. 5, the arm support points are relatively close to each other even with widely different sizes and weights of a user. The arm support point for the 5th percentile female

TABLE 1. Various parameters for different percentiles (PCTL) of males and females. These include: arm length from the shoulder to the wrist (Arm Length); distance from the elbow to the arm support point (Forearm Support Dist.); and upward force required at the arm support point to provide gravity compensation for the arm (Arm Support Force). The arm lengths are taken from [47], and the forearm support distance and arm support force are calculated using values from [47]–[49].

	Males			Females		
PCTL	Arm Length (cm)	Forearm Support Dist. (cm)	Arm Support Force (N)	Arm Length (cm)	Forearm Support Dist. (cm)	Arm Support Force (N)
5th	73.7	17.1	21.8	66.9	15.5	17.8
50th	80.3	18.7	30.5	73.5	17.2	25.2
95th	87.7	20.5	44.9	80.7	18.8	40.3

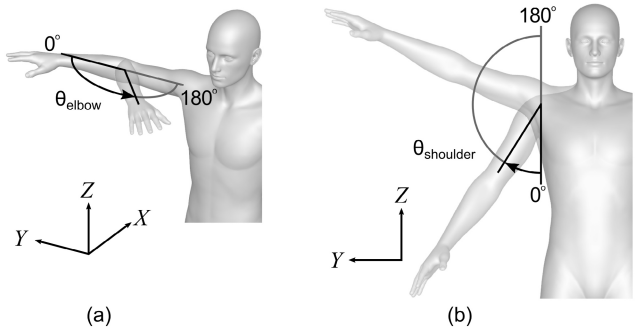

FIGURE 6. (a), Transverse plane elbow sweep. (b), Frontal plane shoulder sweep.

(50.2 kg, 1.50 m tall) and 95th percentile male (124.1 kg, 1.88 m tall) are only 5 cm away from each other, suggesting that the geometry of an exoskeleton could be possibly kept constant on the forearm and fit all users. Of course, the upward force required varies substantially between these different users, as specified in Table 1.

Also drawn on this figure is the geometry of our Panto-Arm exoskeleton (thin gray lines). Our exoskeleton was not optimized when it was designed, and supports the forearm at a point much closer to the elbow than any of the biological arm support points.

2) OVERVIEW OF SWEEP SIMULATIONS

The forces exerted by the Panto-Arm exoskeleton were simulated for two different arm motion sweeps, as shown in Fig. 6. For the two arm sweeps it is assumed that only three forces act on the exoskeleton: a downward force at the fulcrum created by the webbing strap, an upward force at the arm pantograph point generated by a gas spring, and the reaction force at the arm pantograph point. In the model, all of the arm weight is supported at the shoulder joint and the arm support point at the center of the forearm cuff. This is a simplification of the exoskeleton, as in reality some forces are transmitted between the upper arm cuff and the arm.

The first arm sweep, which we refer to as a “transverse plane elbow sweep,” (Fig. 6(a)) is with the arm remaining in a shoulder-height plane parallel to the transverse plane. The upper arm remains pointed to the side from the torso parallel to the frontal axis, and the elbow extends from 0° (fully extended) to 150° (fully flexed), remaining in the plane.

The second arm sweep, which we refer to as the "frontal plane shoulder sweep," (Fig. 6(b)) is with the arm straight (elbow fully extended) and always in the frontal plane. The shoulder moves from 0° (fully adducted) to +180° (fully abducted).

The values for the variables used in the simulations were set to correspond to the lengths of our exoskeleton when it was adjusted to fit one of the researchers. The simulated pantograph ratio is the same as the exoskeleton ($R = 6$). All simulations were performed using MATLAB (The MathWorks, Inc., Natick, MA, USA).

In the simulations, a gas spring was used with a force according to (4), which is taken from [50]. In the equation, F_{spring} is the force of the gas spring for a displacement (stroke) of s, F_{init} is the initial (uncompressed) force of the gas spring, F_{end} is the maximum (fully compressed) force of the gas spring, and s_{max} is the maximum stroke. The gas spring parameters were determined by the spring used in the physical design: $F_{init} = 133.4$ N and $F_{end} = 169.0$ N.

$$F_{spring}(s) = F_{init} \cdot \left(\frac{s_{max}}{s_{max} - s \cdot \left(1 - \frac{F_{init}}{F_{end}}\right)} \right) \tag{4}$$

3) TRANSVERSE PLANE ELBOW SWEEP

The basic geometry of the exoskeleton for the transverse plane elbow sweep is shown in Fig. 5. Forces are applied at the fulcrum, arm pantograph point, and arm support point. The directions of the forces at the fulcrum and arm pantograph point are determined by the positions of both the top and bottom of the webbing and gas spring, and thus are not perfectly vertical. Additionally, these forces are not directly applied to points in-plane with the four bar linkage, but are offset below the main links as with the real device.

Fig. 7 shows how the vertical and lateral force output at the arm support point changes as the position of the lower end of the webbing strap is adjusted laterally from a zero-point that sits beneath the pantograph elbow, as shown in the inset. The curves corresponding to our Panto-Arm Exo's geometry are shown by a black dashed line.

4) FRONTAL PLANE SHOULDER SWEEP

Simulations were also performed for the frontal plane shoulder sweep. The exoskeleton was simplified to the vector representation of the geometry shown in Fig. 8. The representation maintains the positions of the webbing strap, gas spring, fulcrum, arm pantograph point, and arm support point, while simplifying the four bar linkage. The lower ends of the webbing strap and gas spring are referred to as the "webbing base" and "gas spring base," respectively. Because the elbow never bends for the frontal plane shoulder sweep, the planar linkage bars are restrained to be in-line. These bars are labeled the "arm base," which is the top of the planar four bar linkage on which the arm rests. Additionally, the location of the shoulder is specified. Note that in the diagram, the line connecting the fulcrum and arm pantograph point is labeled

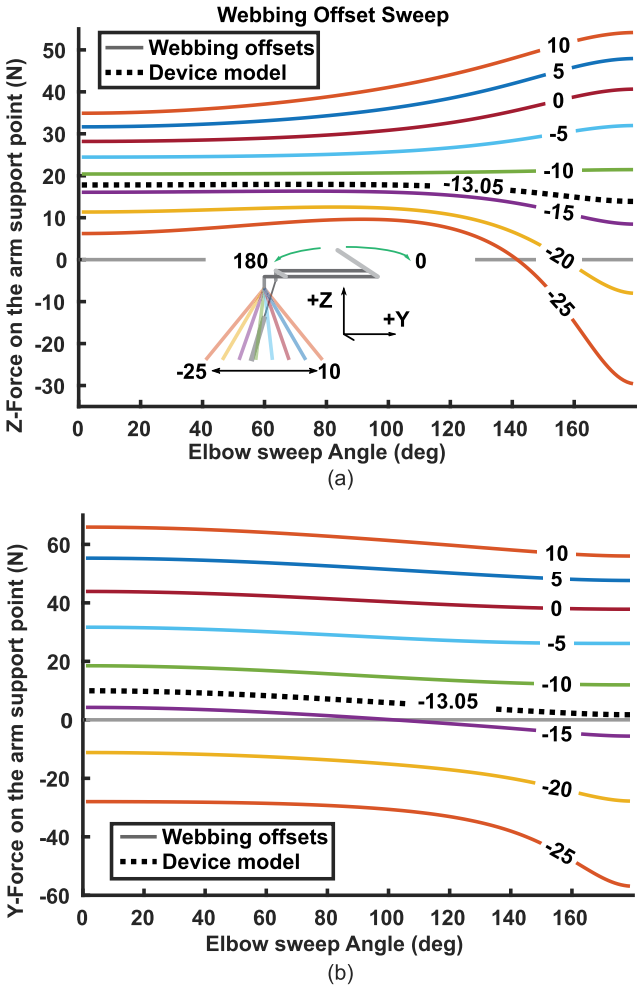

FIGURE 7. Results from the transverse plane elbow sweep of a Class 3 pantograph exoskeleton, where the lower end of the webbing is moved horizontally. Numbers on the lines indicate locations of the lower end of the webbing strap, in centimeters. The zero position lies directly below the pantograph elbow joint. (a) shows support point force in the upwards vertical, or $+Z$, direction, while (b) shows support point force in the $+Y$ or lateral direction.

the "exoskeleton balancing line" instead of the "arm balancing line," because it is at an angle with respect to with the biological arm, as occurs with the actual exoskeleton. For each of the simulations, the bar lengths and various offsets were matched to those of the actual exoskeleton, except as specified.

In each frontal plane sweep, the shoulder angle $\theta_{shoulder}$ is varied from 0° to 180°, following the angle conventions in Fig. 6. The arm and exoskeleton structure attached to the arm rotate about the shoulder point for each value of $\theta_{shoulder}$, and the resulting forces at the arm support point are calculated. To understand how the different parameters affect the resulting forces at the arm support point, sensitivity analyses were done for select parameters.

Fig. 9 shows the effect of altering the angle of the exoskeleton balancing line relative to the arm base, as shown in the inset on the figure. In this simulation, we consider both a realistic gas spring as well as one with a potentially

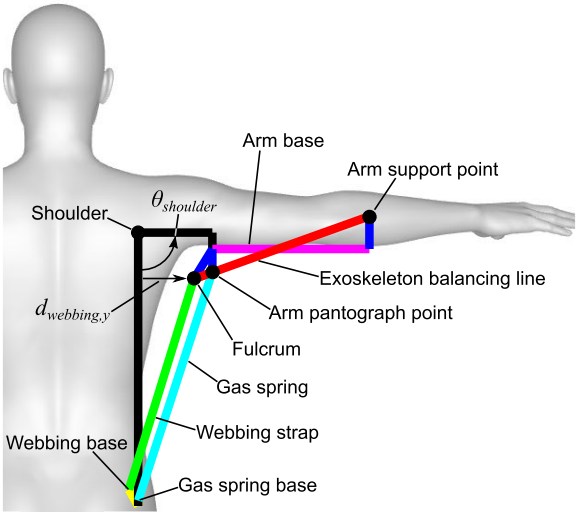

FIGURE 8. Representation of the exoskeleton for the frontal plane shoulder sweep simulations.

infinite travel. Gas springs have physical limitations preventing over-extension and over-compression; in the figure, dark lines indicate curves corresponding to the physical travel limits of the gas spring, and lighter lines show the force outputs following the same gas spring equation but without restrictions on the travel distance. As can be seen, this variable influences both the magnitude of the forces in the Y and Z directions, as well as the location of the peak force.

The exoskeleton was also evaluated by manipulating the Y-distance from the webbing point to the side of the user, $d_{webbing,y}$, with the results in Fig. 10. This is analogous to a constant-sized exoskeleton being worn by users with different arm lengths: with the exoskeleton elbow aligned with the wearer's elbow, the fulcrum and arm support point lie closer to or further from the wearer's torso. As can be seen in the figure, the resulting curves are nearly overlapping, indicating that displacing the exoskeleton laterally from the shoulder has a minimal effect on its output forces.

Fig. 11 shows the effect of moving the webbing base point horizontally relative to the gas spring base point. Changing this effectively manipulated the angle of the webbing with respect to vertical, which in turn influences how much of the force on the arm support point is in the Y versus Z directions. In this sweep, $d_{webbing,y}$ is set to be -2.5 cm (to the left of the shoulder in Fig. 8), which simulates the exoskeleton being located somewhat behind the body, and the exoskeleton balancing line parallel to the arm base an in line with the shoulder, keeping all other device parameters consistent with the actual exoskeleton. The results show that the slope of the force in the Z-direction is strongly influenced by this value, while in the Y-direction the curves maintain approximately the same shape but translate vertically.

B. TOOL SUPPORT EXOSKELETON ANALYSIS

We also simulated a Class 1 pantograph exoskeleton similar to our Panto-Tool Exo, using a model similar to that in Fig. 8.

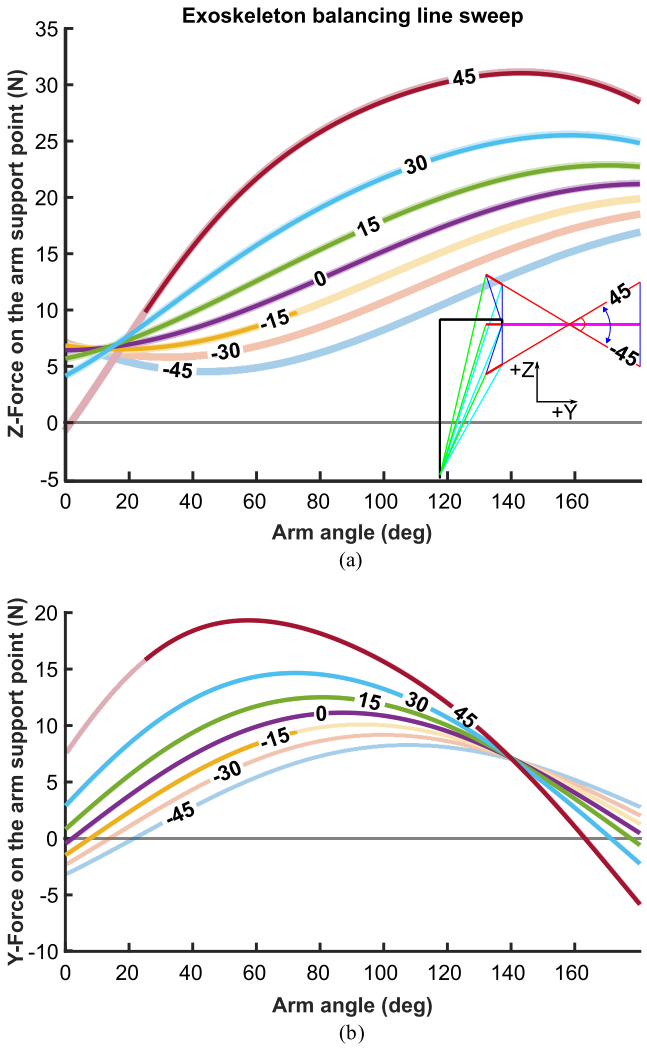

FIGURE 9. Results from frontal plane shoulder sweep, with the angle of the exoskeleton balancing line relative to the arm base varied. Numbers on the lines are the inclination angle in degrees, as indicated in the inset. The darker portions of the lines correspond to the gas spring length being within a physical range, while lighter lines correspond to theoretical behavior following the same gas spring force equation. (a) shows force in the *Z* or craniocaudal axis, while (b) shows force in the *Y* or frontal axis.

As compared to the model in Fig. 8, in the Class 1 device the fulcrum location is fixed and aligned with the shoulder, whereas in the Class 3 device the gas spring extends and compresses. Here, the exoskeleton was configured to support the weight of a tool in the user's hand, and simulated with a constant force of 600 N pulling down on the tool pantograph point (corresponding to a tool support force of 100 N, chosen to be a round number). The force on the tool pantograph point is simulated to always pull in the direction of a fixed "pulley point," which could be the location of a physical pulley with a cord passing through it.

Unlike a rigid lever, where any horizontal forces could be supported by the fulcrum, leaving the tool forces to be purely vertical, in our simulation we have no horizontal forces at the fulcrum along the axis between the tool pantograph point and tool support point (the tool balancing line).

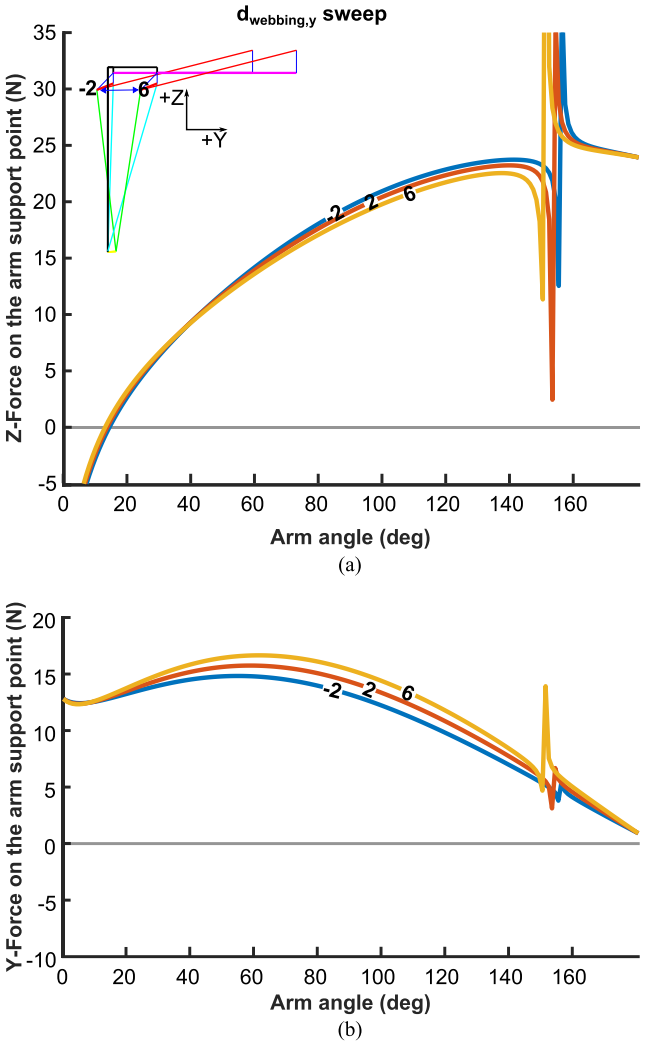

FIGURE 10. Results from a frontal plane shoulder sweep when the horizontal location of the fulcrum (top of the webbing strap) is varied with respect to the shoulder ($d_{webbing,y}$ in Fig. 8). Numbers on the lines correspond to values of $d_{webbing,y}$ in cm. Negative values correspond to when the fulcrum is located medial to the shoulder. (a) shows force in the *Z* or craniocaudal axis, while (b) shows force in the *Y* or frontal axis.

This is because, due to the four bar linkage, the distance between the tool pantograph point and the tool support point can change. Horizontal forces between the fulcrum and the tool pantograph point will serve to collapse the four bar linkage at the elbow joint. Thus, even though the fulcrum is fixed with respect to the body, all of the horizontal forces must be supported by the tool (or by the arm at the location of the tool). All of the values used in this simulation were measured from the built version of the exoskeleton as a Class 1 lever shown in Fig. 1.

Fig. 12 shows the results of moving the pulley point laterally, similarly to the simulation in Fig. 11 for the Class 3 exoskeleton. The resulting curves appear similar, with small differences in the shape of the curves due to the gas spring's motion and the non-constant force created by the gas spring in the Class 3 simulation, as compared to the fixed fulcrum and constant force magnitude in this simulation.

The Class 1 exoskeleton geometry was also optimized for flatness of the tool force in the *Z* direction, with the resulting force curves for both the frontal plane shoulder sweep and transverse plane elbow sweep shown in Fig. 13. The results have a maximum of 10% variation in the *Z*-force over the range of 45° to 135° in the frontal plane sweep. In Fig. 13(b), note that while we simulate the transverse plane elbow sweep up to an elbow angle of 180°, in practice people are only able to bend their elbows to roughly 150°. In order to achieve flatter tool force curves, the force supplied to the pantograph arm would need to be non-constant, or a different mechanism would be needed to keep the force more vertical. Fig. 13 also shows the results for a force that is kept perfectly vertical (dashed lines). These can be seen to provide the nominal behavior for the linkage, and results in a gravity compensation force that is purely vertical with a constant magnitude.

IV. METHODS

A. MECHANICAL EVALUATION

In order to validate our simulations, we conducted experiments to measure the Panto-Arm Exo's force. The forces created by the exoskeleton were measured by a force torque sensor (ATI Industrial Automation FT13186 Net Force Torque sensor) as it was moved through the same sweeps as the simulations discussed above and as shown in (Fig. 6). The sensor was mounted to the exoskeleton with the center of the sensor (where forces and torques are measured) positioned at the location where the center of the arm would lie. The plate on the exoskeleton waist belt was mounted to a fixture. Researchers moved the exoskeleton to a prescribed position, then collected force/torque data with a mouse click. This was repeated five times for each position, and the data were averaged. Since the sensor was mounted to the exoskeleton and rotated as the elbow or shoulder angle was varied, a coordinate transformation was performed to put the forces in the global coordinates.

B. ELECTROMYOGRAPHY

A study was also completed to understand how the Panto-Arm exoskeleton affects the activation of a wearer's arm muscles, using surface electromyography (EMG). The study used a sample of 12 healthy people, including 5 females and 7 males. The participants had a mean (standard deviation) mass of 79.6 (16.4) kg, height of 178 (12) cm, and age of 23.3 (3.7) years. The study was approved by the Institutional Review Board (IRB) of Virginia Tech (IRB # 19-074) and all participants signed consent forms at the beginning of the study session. None of the participants had a history of musculoskeletal disorders relating to their arms and all participants were able to comfortably lift 2.27 kg (5 lbs).

The EMG sensors used were the wireless Delsys Trigno system (Delsys Inc., Boston, MA, USA) which has a sampling frequency of 1925.93 Hz, a bandwidth of 25-450 Hz, and a differential gain of 1000. The muscles tested were

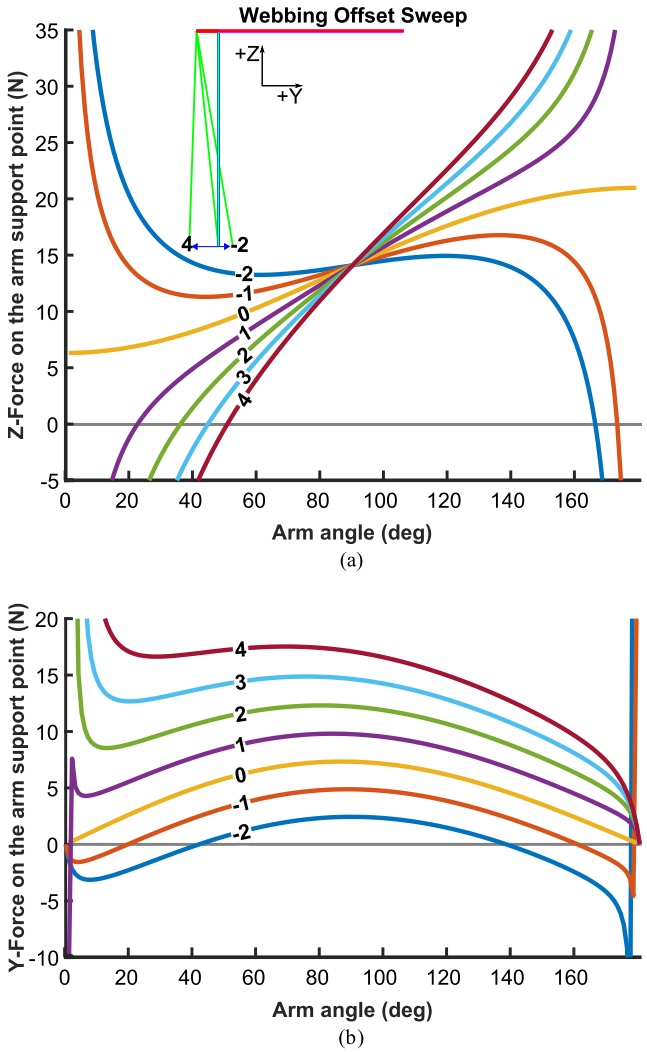

FIGURE 11. Results from frontal plane shoulder sweep when the location of the lower end of the webbing is varied horizontally. The value of zero corresponds to the webbing being located under the arm pantograph point when the shoulder is at 90°. The plots show the forces on the arm support point. Subfigure (a) shows force in the *Z* or craniocaudal axis, while subfigure (b) shows force in the *Y* or frontal axis.

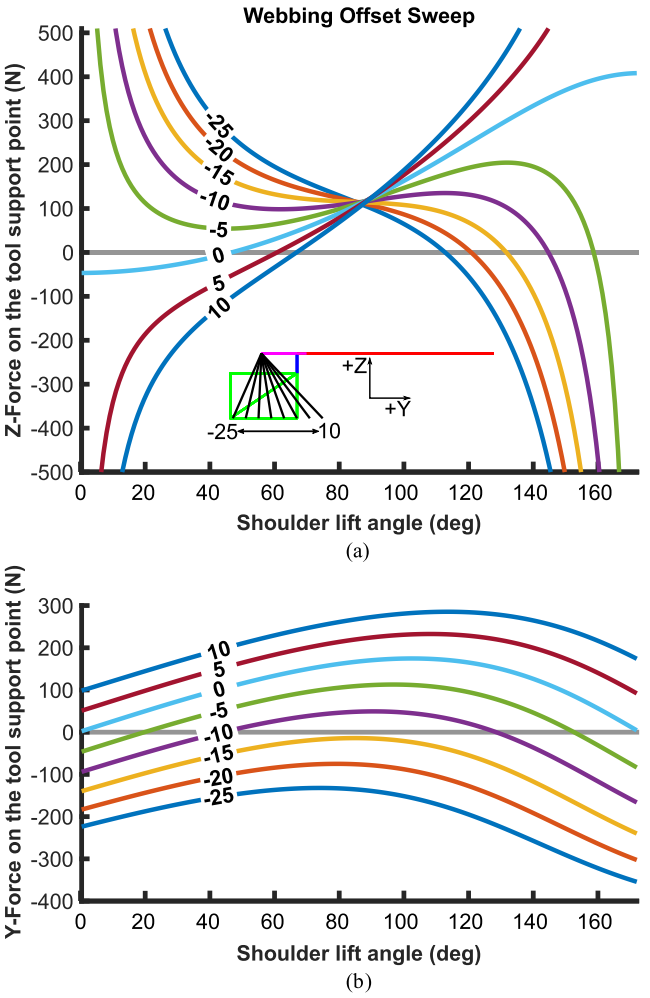

FIGURE 12. Simulation of the exoskeleton configured as a Class 1 lever with a constant force on the webbing. The graph shows the force on the tool as the shoulder lift angle is varied in a frontal plane shoulder sweep. Different curves correspond to different locations of the lower end of the webbing, as shown in the inset. (a) shows force in the *Z* or craniocaudal axis, while (b) shows force in the *Y* or frontal axis.

the Mid Deltoid (also known as Lateral Deltoid), the Biceps Brachii, the Brachioradialis, and the Wrist Flexor (Flexor Carpi Radialis), as shown in Fig. 14(c). The methods for placing the EMG sensors were found from Seniam for the Mid Deltoid [51] and Thought Technology for the Biceps Brachii, Brachioradialis, and Wrist Flexor [52].

1) PREPARATION

All of the participants were fit to the exoskeleton prior to putting on the EMG sensors. The fitting process started with placing the base of the gas spring in line with the hip, rotated towards the rear by about 5 cm. There were two pad thicknesses (1 and 2.25 cm) which were used on the arm cuffs based on user preference. Typically participants with thinner arms preferred the thinner of the two pad options. Next, the exoskeleton was adjusted by shifting the waist belt relative to their torso and pelvis, both up/down and left/right, so that the participant could move their arms through all of the motions of the study and still feel comfortable and supported by the exoskeleton. The webbing strap was also tightened or loosened to maximize user comfort and mobility.

2) EXPERIMENTAL PROCEDURE

The participants performed Maximum Voluntary Contraction (MVC) measurements for each muscle. For the Mid Deltoid, participants sat parallel to the table, placed their arm to their side with their elbow bent at a 90° angle, and aligned their forearm with the edge of the table. They then pushed laterally away from the body and into the table. The MVC for the Brachioradialis, Biceps Brachii, and the Wrist Flexor were all done in one test. The participants faced the table while seated and aligned their wrist with the edge of the underside of the table, such that their elbows were supported by the chair. The participants then pushed up on the table, attempting to curl both their wrist and forearm upward. Both

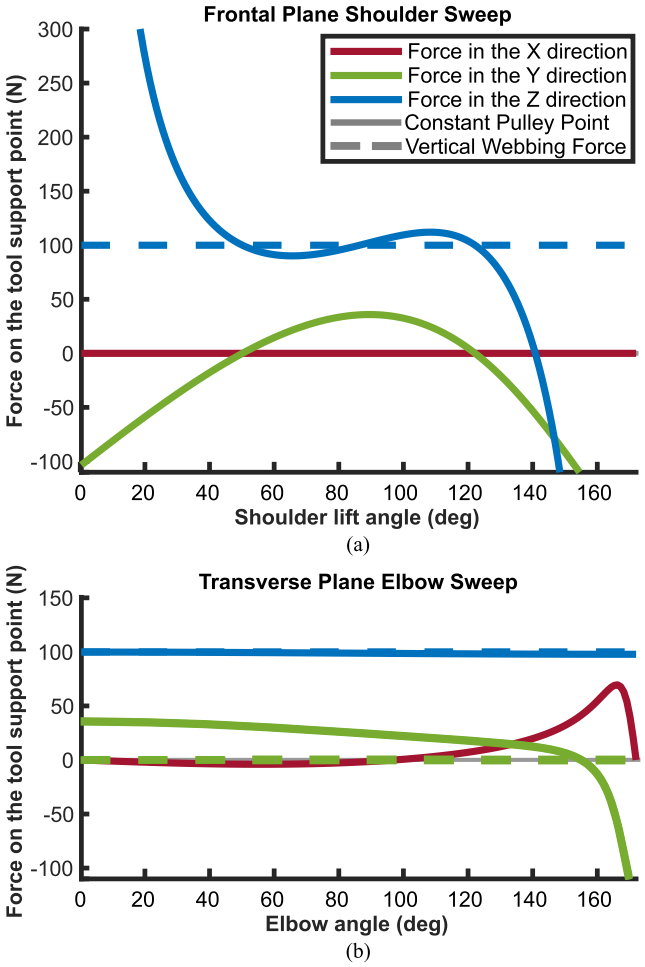

FIGURE 13. Simulation of the exoskeleton configured as a Class 1 lever with a constant force on the webbing and the geometry optimized for flat force curves. Each graph shows the force on the tool in the the *X*, *Y*, and *Z* directions, with solid lines corresponding to a fixed pulley location and dashed lines corresponding to forces on the tool pantograph point that are always vertical. (a) shows the forces for the frontal plane shoulder sweep, while (b) shows the forces for the transverse plane elbow sweep.

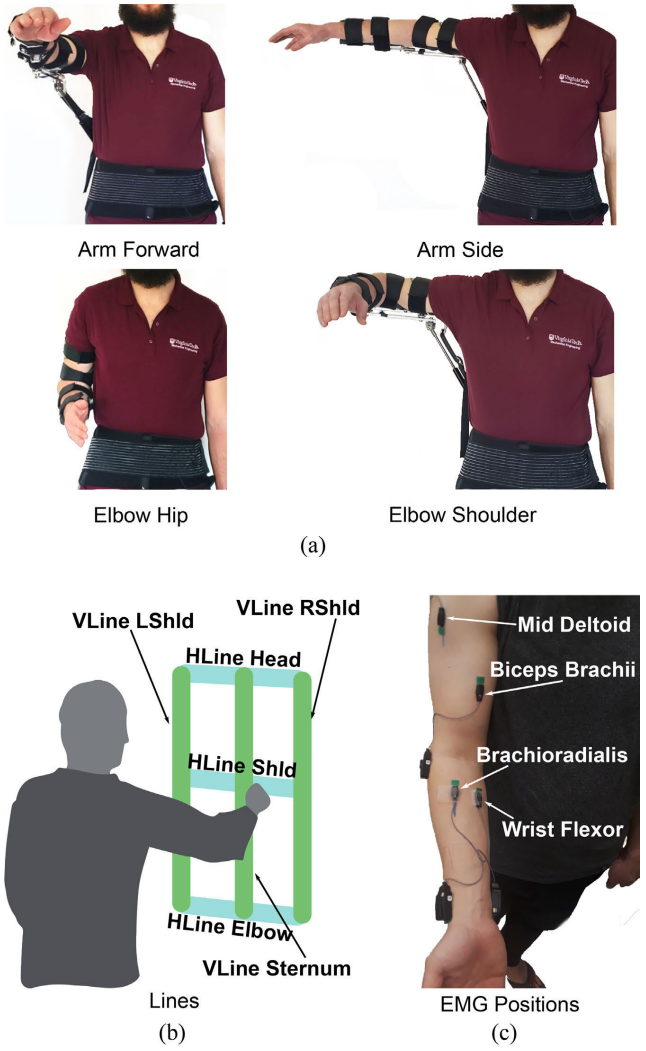

FIGURE 14. (a), static postures used when measuring the EMG signals; (b), illustration of the motions used when measuring the EMG signals during dynamic tests. "VLine" stands for a vertical line, "HLine" stands for a horizontal line, and "LShld"/"RShld" stand for the lines positioned at the left and right shoulders, respectively. (c), locations of the EMG electrodes.

MVC tests were repeated twice and each test took 4 seconds with the participants receiving verbal cues to ramp up to and back down from their maximum muscle activation.

The participants then performed static and dynamic tasks with and without the exoskeleton. The tasks and exoskeleton assistance were randomized according to Latin square principles to reduce systematic error. The tests were broken into static and dynamic tests with 20 seconds of rest provided between each experimental condition.

The static tests all involved holding an arm position for 4 seconds repeated with and without a mass of 2.27 kg (5 lbs.) held in the hand; the participants were asked to relax their wrists for all of the positions. The static tasks were done with postures as shown in Fig. 14(a). In the Arm Forward posture, the participant held their arm in front of them, parallel to the ground, at shoulder height. In the Arm Side posture, the participant held their arm to the side of their chest, parallel to the ground, and at shoulder height. In the Elbow Shoulder posture, the participant held their arm similarly to the Arm Side position but with the forearm perpendicular to the upper arm, and in the Elbow Hip posture the participant held their elbow beside their hip, with their forearm parallel to the ground.

The dynamic tests involved drawing horizontal and vertical lines on a white board, illustrated in Fig. 14(b). The participants first stood with their arms extended and palms flat on the whiteboard to standardize the distance away relative to arm length. The horizontal line tasks consisted of drawing shoulder-width horizontal lines at the top of the head, shoulder, and elbow heights for each participant. The horizontal line tasks were performed for 7 seconds with a shoulder-to-shoulder time of roughly one second. The vertical line tasks consisted of top-of-the-head to elbow height vertical lines at the subject's left shoulder, sternum, and right shoulder. The vertical line tasks were performed for 15 seconds with a top to bottom time of roughly two seconds. A 60 bpm metronome

was played to help the participants with timing for the line tasks.

3) DATA PROCESSING

The EMG data was processed using MATLAB and then transferred into JMP Pro 15 (SAS, Cary, NC) for statistical analysis. The EMG signal was first sent through a 6th order band pass Butterworth filter with a frequency band of 20-450 Hz, then a notch filter to remove any 60 Hz noise. The data was rectified, followed by a low pass filter with a 3 Hz cutoff to smooth the data. For each test case the mean of the data was taken and divided by the maximum MVC values for each of the muscles. Two and three factor repeated measures analysis of variance (ANOVA) was performed with an alpha value cut off of 0.05. The three independent variables investigated with this study were Task Performed, Mass held (for static tests only), and Exoskeleton Assistance.

V. RESULTS

A. MECHANICAL LINKAGE MEASUREMENTS

Fig. 15 shows the results of the Panto-Arm Exo measurements. Fig. 15(a) shows the response to the shoulder sweep in the frontal plane. The Arm Side position of the EMG experiments is shown with a 5 degree band on the graph. Fig. 15(b) shows the response to the elbow sweep in the transverse plane. For reference, the Elbow Shoulder and Arm Side positions of the EMG experiments are shown with a 5 degree band on the graph. In each of these graphs, each experimental data point represents the average of five measured data points.

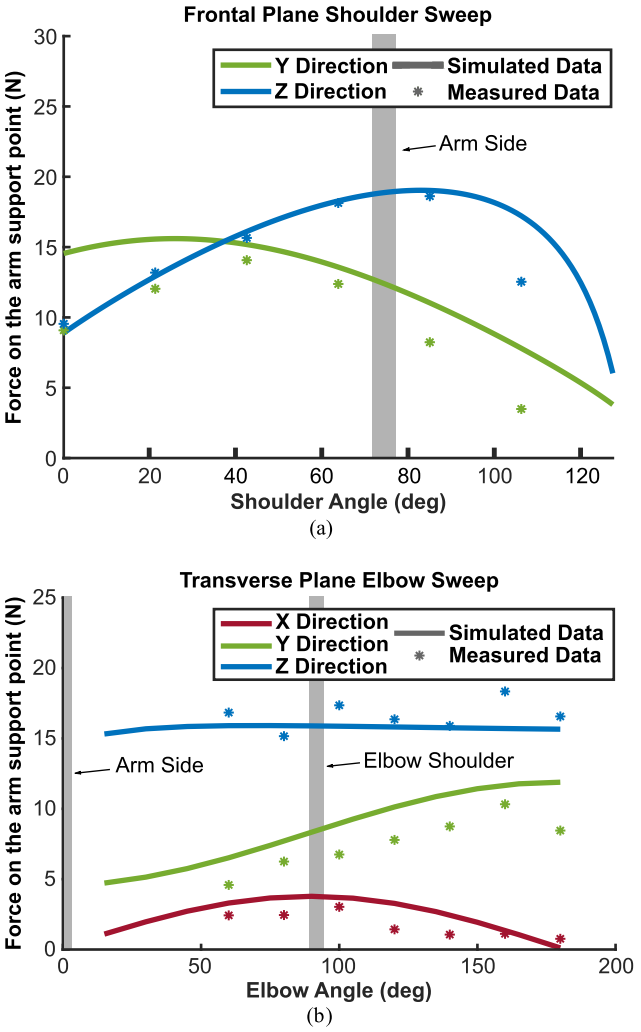

FIGURE 15. Experimental results for our Panto-Arm exoskeleton as compared to simulations. (a) shows the shoulder sweeping through the frontal plane, and (b) shows the elbow sweeping through the transverse plane. For both, gray bars show where the exoskeleton's angles corresponded to the positions measured in the EMG experiment.

B. EMG RESULTS

Fig. 16 shows results for normalized muscle activation with and without the exoskeleton during the static tests. While collectively looking at all the static tests and both masses, both the Mid Deltoid and the Biceps Brachii showed a statistically significant decrease in muscle activation while wearing the exoskeleton ($p<0.0001$ and $p=0.0097$ respectively). Exoskeleton Assistance did not create a significant change for either the Wrist Flexor or the Brachioradialis. As expected, all four muscles had significantly greater activation while holding the 2.27 kg (5 lbs.) mass as compared to 0 kg.

For the Mid Deltoid, interaction effects between Test and Exoskeleton Assistance show that the greatest decrease from Without-Exoskeleton to With-Exoskeleton (averaged across both masses) occurred during the Arm Forward task (42.9% reduction) followed by Elbow Shoulder (41.2% reduction). The greatest decrease from Without-Exoskeleton to With-Exoskeleton for the Biceps Brachii was during the Arm Forward task (51.9% reduction), closely followed by Arm Side (51.6% reduction). The Elbow Shoulder posture had a slight, but not statistically significant, increase in the Biceps Brachii activation while wearing the exoskeleton.

Fig. 17 shows results for normalized muscle activation with and without the exoskeleton during the dynamic tests. Similar to the static tests, while collectively looking at all the dynamic tests and both masses, both the Mid Deltoid and the Biceps Brachii showed a statistically significant decrease ($p=0.0040$ and $p=0.0020$ respectively) in muscle activation while wearing the exoskeleton. Again, there was no significant change based on Exoskeleton Assistance for the Wrist Flexor and Brachioradialis.

As with the static tasks, the dynamic tasks also had significant interaction effects between Test and Exoskeleton assistance for the Mid Deltoid and the Biceps Brachii. The greatest decrease from Without-Exoskeleton to With-Exoskeleton for the Mid Deltoid was during the horizontal line at shoulder height task (56.5% reduction), followed by the horizontal line at head height (37.0% reduction). For the Biceps Brachii, the greatest change between with and without the exoskeleton

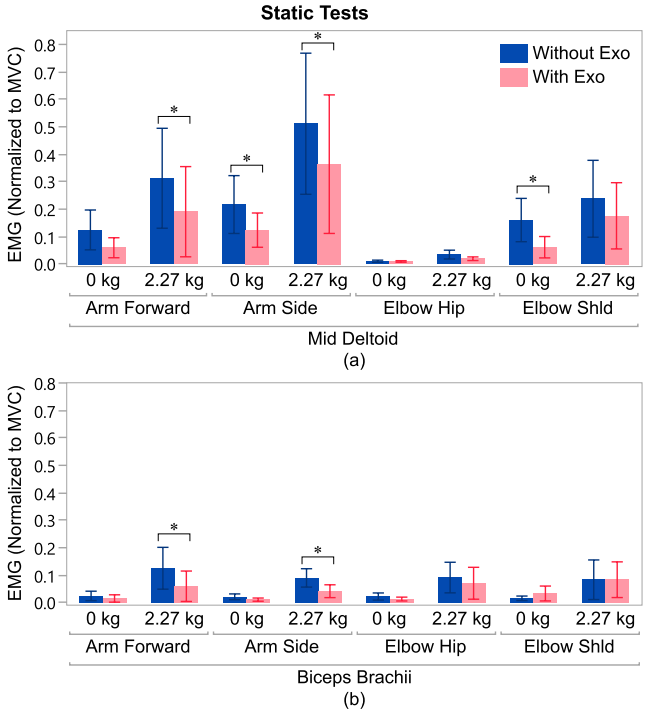

FIGURE 16. Muscle Activation for static tests with the Mid Deltoid and Biceps Brachii. Each error bar is constructed using 1 standard deviation from the mean.The '*' represents statistical significance (p-value < 0.05) between with and without exo condition.

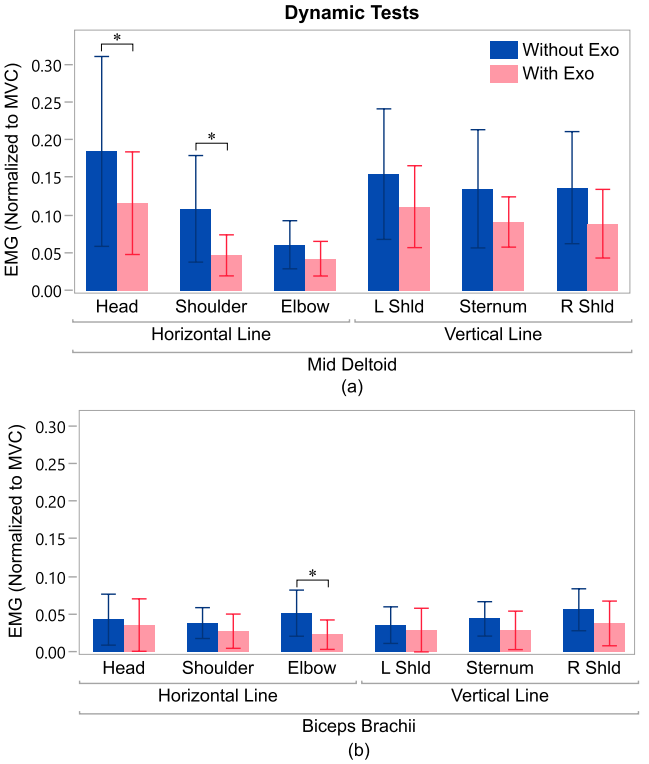

FIGURE 17. Muscle Activation for dynamic tests with the Mid Deltoid and Biceps Brachii. Each error bar is constructed using 1 standard deviation from the mean.The '*' represents statistical significance (p-value < 0.05) between with and without exo condition.

was seen during the horizontal line at elbow height task (54.9% reduction).

VI. DISCUSSION

The mechanical design measurements of the exoskeleton matched the simulation fairly closely. One primary cause of error in the simulation was the assumption of a shoulder point that is uniform throughout the sweeps. On the actual human body the shoulder joint does not have a uniform rotation point but rather a point which itself moves as the shoulder angle changes. The exoskeleton has a floating shoulder point and is able to shift slightly with respect to the arm, which accounts for this non-uniform rotation point. To simplify the simulation, the rotation point and location on the user's arm were assumed to be constant and the webbing was allowed to slightly change height near the user's hip. In the experimental testing, this flexible hip height was duplicated; however, due to the floating shoulder point, perfectly replicating the simulation was challenging in some orientations, especially for the frontal plane shoulder sweep. Another contribution to the difference between the simulated and experimental data is the hysteresis and static friction in the gas spring. This was mitigated by only recording measurements when the gas spring was compressed and not allowed to extend. Finally, the joint where the gas spring connects to the exoskeleton has more degrees of freedom than were modeled in the simulation. Stabilizing the exoskeleton during the experiments led to an increase in moments required for stability and a slight change to the forces.

The parameter sweep simulations indicate that several parameters are important to achieve a flat force profile, while others matter much less. The horizontal distance between the lower ends of the gas spring and webbing strap for the Class 3 exoskeleton (or the horizontal distance between the fulcrum and the bottom of the webbing strap in the Class 1 version) is one of the important parameters (Figs. 11 and 12, respectively). Changing this alters the degree to which the forces on the pantograph point are vertical, which affects the shape of the Z-forces as well as the magnitude of the Y-forces. This parameter is also the only one that substantially affects the arm support point forces in the transverse plane elbow sweep; other graphs of the transverse plane elbow sweep were not shown in the Results section because they did not show substantial changes in the force profiles. In general, the arm support forces in the transverse plane elbow sweep are relatively constant, exhibiting variations of less than ~20% as the elbow moves. This is because as the elbow moves, the arm pantograph point moves relatively little, as the upper arm remains stationary and the forearm's motion is the only component that contributes to the motion of the whole arm center of mass.

The angle between the biological arm and arm support line (Fig. 9) has a moderate impact on the arm support point forces. For small deviations from parallel ($-15°$ to $+15°$), there are relatively small changes in the arm support point forces (within ~ 20%), but these increase at larger angular

deviations. Thus, locating the fulcrum and arm pantograph point close to the upper arm is important, which can be done by making the exoskeleton linkage flatter or providing vertical offsets from the planar linkage to where the gas spring and webbing connect, such that the exoskeleton balancing line is more centered on the arm.

In contrast, adjusting the distance between the exoskeleton and the shoulder joint ($d_{webbing,y}$, with simulation results in Fig. 10) does not cause large changes to the arm support point forces. This indicates that the size of the exoskeleton could be somewhat standardized instead of being custom-built for each user. Similarly, while not specifically swept, the distance between the fulcrum and the biological shoulder joint does not appear to affect the force curves very much. This can be observed by comparing the "0" lines in Figs. 9 and 11. The only difference between these two simulations is the location of the fulcrum with respect to the shoulder, and the two resulting curves are very similar. However, the alignment between the fulcrum and shoulder does affect the exoskeleton's upper travel limit. As can be seen in Fig. 1(b) and Fig. 3, when the shoulder angle reaches around 120°, the exoskeleton reaches a singularity where the gas spring and webbing strap line up with the exoskeleton balancing line. This prevents the arm from raising further. In our Panto-Arm Exo, the maximum shoulder angle is high enough to permit the wearer to touch the top of their head, suitable for most activities of daily living. This could be further improved by positioning the fulcrum somewhat behind the torso, as we did in the Panto-Tool Exo.

Making the forces on the pantograph point more vertical can also be done by other means. In our exoskeletons and simulations the gas spring and webbing strap are mounted to the user's waist, and thus their lengths are determined by the distance between the waist and shoulder. Moving their ends to a position below the waist leads to flatter force curves, but is not practical for an exoskeleton. Alternatively, the lower end of the webbing can be permitted to freely move horizontally with respect to the lower end of the gas spring (Class 3 Exo) or fulcrum (Class 1 Exo). This could be accomplished by connecting the webbing to a structure with several short links in series, connected by joints that revolve around the vertical axis to that the end of the last link can move in the horizontal plane. Alternatively, a parallelogram linkage with an extension spring on the diagonal could be used, as was studied in [12]. This structure generates a constant force, and if the length of the parallelogram's top link is equal to the average length of the pantograph arm, the parallelogram will change the radius from the fulcrum as it moves up and down. While this would not accommodate the motion of the elbow, it would make the forces on the webbing substantially more vertical. It can be seen in Fig. 13 that if the forces on the webbing are perfectly vertical, then indeed the pantograph works as expected and produces constant forces independent of the arm's motion. One possible extension to this work is to use a motor to actively move the pulley point on a Class 1 exoskeleton to different locations in the sagittal plane, e.g. up and down the wearer's back [42]. In this manner, the force vectors on the webbing could be directed to be in a different direction than vertical. This could allow the forces on the arm or tool to remain parallel to the gravity vector, even as the wearer tilts their torso forward.

Alternatively, it may be beneficial in some cases to have the forces on the arm or tool support point not be perfectly vertical. For a tool-support exoskeleton, a small bias force pulling the tool towards the wearer may help them control the tool more effectively. Or, in a stroke rehabilitation application, a small bias force extending the elbow may be beneficial if a wearer has difficulty doing this themselves.

The EMG results matched our expectations fairly well. The Panto-Arm Exo supports both the upper arm and the forearm directly but does not support the hand; as such, we expected a reduction in the muscles which support the upper arm and forearm, but no change in the muscles that support the hand. The EMG results showed that the Mid Deltoid and Biceps Brachii had reductions for most of the postures and motions evaluated. The Mid Deltoid is positioned on the shoulder, supporting the whole arm, and the Biceps Brachii is positioned on the upper arm and supports the forearm. In contrast, the Brachioradialis and Wrist Flexor muscles showed little change comparing With- and Without-Exoskeleton assistance, as expected.

The EMG results are also quite promising because the exoskeleton used for testing was not optimized. The arm support point was much closer to the elbow than desired (Fig. 5), and the magnitude of the force at the arm support point was roughly half of the force to support the arm ($\sim$ 16 N vs. 25-30 N for 50th percentile males and females, as seen in Table 1). Additionally, the linkage geometry resulted in non-constant forces that were sometimes pushing the forearm away from the body (Fig. 15). Even with these imperfections, the exoskeleton still resulted in reductions in the Mid Deltoid of 42% in several postures, and reductions in the Biceps Brachii of more than 50% in the Arm Forward and Arm Side postures.

In the dynamic tests, the Mid Deltoid showed statistically significant reductions for the horizontal line tasks at head and shoulder heights, with similar magnitudes to the static tests (37-57% reductions). The Biceps Brachii only showed a significant reduction for the horizontal line at elbow height (55% reduction). These motions were a useful first evaluation of the exoskeleton, but an expanded set of motions could better represent how the arm is used during activities of daily living.

VII. CONCLUSION

We presented a new method for gravity compensation of a human or robot arm, and demonstrated it with two exoskeletons. Compared to previous work, these exoskeletons uniquely follow the kinematics of the wearer's arm, and our Panto-Arm exoskeleton is low-profile enough to fit under a jacket. The concept for gravity compensation works as desired, but is somewhat sensitive to the direction of the

forces applied to the fulcrum and pantograph points. The exoskeletons presented in this article were not optimized; future work can be done to improve the force production mechanisms and means of keeping the forces parallel to the gravity vector. Finally, it would be useful to conduct future work on evaluating these exoskeletons in rehabilitation or in workplace environments.

ACKNOWLEDGMENT

The authors would like to thank Andrew Bolkhovitinov, Anna Murgia, Christopher Gavan, Cindy Chang, Emily Schanz, Josh Wenger, Julian Park, Lana Volchematieva, Lenna Roman, Michelle Prisbe, and Pat Girvan for their assistance in fabricating early versions of the exoskeletons, and Jack Duffin, Nathan Folta, and Erin Smith for assistance in fabricating the recent versions.

REFERENCES

[1] Ekso Bionics. (2020). *EksoVest Product Page*. Accessed: Jul. 15, 2020. [Online]. Available: https://eksobionics.com/eksoworks/eksovest/
[2] US Bionics. (2017). *ShoulderX by SuitX Product Page*. Accessed: Jul. 15, 2020. [Online]. Available: http://www.suitx.com/shoulderx
[3] Ottobock SE & Co. KGaA. (2020). *Paexo Product Page*. Accessed: Jul. 15, 2020. [Online]. Available: https://paexo.com/paexo-shoulder/?lang=en
[4] P. Maurice, J. Čamernik, D. Gorjan, B. Schirrmeister, J. Bornmann, L. Tagliapietra, C. Latella, D. Pucci, L. Fritzsche, S. Ivaldi, and J. Babič, "Evaluation of PAEXO, a novel passive exoskeleton for overhead work," *Comput. Methods Biomech. Biomed. Eng.*, vol. 22, no. 1, pp. S448–S450, Oct. 2019.
[5] Levitate Technologies. (2020). *Levitate AIRFRAME Product Page*. Accessed: Jul. 15, 2020. [Online]. Available: https://www.levitatetech.com/
[6] J. Theurel, K. Desbrosses, T. Roux, and A. Savescu, "Physiological consequences of using an upper limb exoskeleton during manual handling tasks," *Appl. Ergonom.*, vol. 67, pp. 211–217, Feb. 2018.
[7] R. Altenburger, D. Scherly, and K. S. Stadler, "Design of a passive, iso-elastic upper limb exoskeleton for gravity compensation," *ROBOMECH J.*, vol. 3, no. 1, pp. 1–7, Dec. 2016.
[8] K. Huysamen, T. Bosch, M. de Looze, K. S. Stadler, E. Graf, and L. W. O'Sullivan, "Evaluation of a passive exoskeleton for static upper limb activities," *Appl. Ergonom.*, vol. 70, pp. 148–155, Jul. 2018.
[9] Lockheed Martin Corporation. (2020). *FORTIS Product Page*. Accessed: Jul. 15, 2020. [Online]. Available: https://www.lockheedmartin.com/en-us/products/exoskeleton-technologies/industrial.html
[10] S. Alabdulkarim and M. A. Nussbaum, "Influences of different exoskeleton designs and tool mass on physical demands and performance in a simulated overhead drilling task," *Appl. Ergonom.*, vol. 74, pp. 55–66, Jan. 2019.
[11] Ekso Bionics. (2020). *EksoZeroG Product Page*. Accessed: Jul. 15, 2020. [Online]. Available: https://eksobionics.com/eksoworks/eksozerog/
[12] T. Rahman, R. Ramanathan, R. Seliktar, and W. Harwin, "A simple technique to passively gravity-balance articulated mechanisms," *J. Mech. Des., Trans. ASME*, vol. 117, no. 4, pp. 655–657, 1995.
[13] L. A. Van der Heide, B. van Ninhuijs, A. Bergsma, G. J. Gelderblom, D. J. van der Pijl, and L. P. de Witte, "An overview and categorization of dynamic arm supports for people with decreased arm function," *Prosthetics Orthotics Int.*, vol. 38, no. 4, pp. 287–302, Aug. 2014.
[14] T. Haumont, T. Rahman, W. Sample, M. M. King, C. Church, J. Henley, and S. Jayakumar, "Wilmington robotic exoskeleton: A novel device to maintain arm improvement in muscular disease," *J. Pediatric Orthopaedics*, vol. 31, no. 5, pp. e44–e49, 2011.
[15] Saebo. *SaeboMAS Product Page*. Accessed: Jul. 15, 2020. [Online]. Available: https://www.saebo.com/shop/saebomas/
[16] P. N. Kooren, A. G. Dunning, M. M. H. P. Janssen, J. Lobo-Prat, B. F. J. M. Koopman, M. I. Paalman, I. J. M. de Groot, and J. L. Herder, "Design and pilot validation of A-gear: A novel wearable dynamic arm support," *J. Neuroeng. Rehabil.*, vol. 12, no. 1, p. 83, Dec. 2015.
[17] B. Mastenbroek, E. de Haan, M. van den Berg, and J. L. Herder, "Development of a mobile arm support (Armon): Design evolution and preliminary user experience," in *Proc. IEEE 10th Int. Conf. Rehabil. Robot.*, Jun. 2007, pp. 1114–1120.
[18] P. Lucieer and J. L. Herder, "Design of an adjustable compensation mechanism for use in a passive arm support," in *Proc. 29th Mech. Robot. Conf., A B*, vol. 7, Jan. 2005, pp. 1–10.
[19] B. E. Perry, E. K. Evans, and D. S. Stokic, "Weight compensation characteristics of Armeo Spring exoskeleton: implications for clinical practice and research," *J. Neuroeng. Rehabil.*, vol. 14, no. 1, pp. 1–10, 2017.
[20] A. H. A. Stienen, E. E. G. Hekman, F. C. T. Van der Helm, G. B. Prange, M. J. A. Jannink, A. M. M. Aalsma, and H. Van der Kooij, "Freebal: Dedicated gravity compensation for the upper extremities," in *Proc. IEEE 10th Int. Conf. Rehabil. Robot.*, Jun. 2007, pp. 804–808.
[21] G. Spagnuolo, M. Malosio, A. Scano, M. Caimmi, G. Legnani, and L. M. Tosatti, "Passive and active gravity-compensation of LIGHTarm, an exoskeleton for the upper-limb rehabilitation," in *Proc. IEEE Int. Conf. Rehabil. Robot. (ICORR)*, Aug. 2015, pp. 440–445.
[22] K. A. Wyrobek, E. H. Berger, H. F. M. Van der Loos, and J. K. Salisbury, "Towards a personal robotics development platform: Rationale and design of an intrinsically safe personal robot," in *Proc. IEEE Int. Conf. Robot. Autom.*, May 2008, pp. 2165–2170.
[23] N. Ulrich and V. Kumar, "Passive mechanical gravity compensation for robot manipulators," in *Proc. IEEE Int. Conf. Robot. Autom.*, Apr. 1991, pp. 1536–1541.
[24] T. Morita, F. Kuribara, Y. Shiozawa, and S. Sugano, "A novel mechanism design for gravity compensation in three dimensional space," in *Proc. IEEE/ASME Int. Conf. Adv. Intell. Mechatronics (AIM)*, Jul. 2003, pp. 163–168.
[25] S. K. Agrawal, G. Gardner, and S. Pledgie, "Design and fabrication of an active gravity balanced planar mechanism using auxiliary parallelograms," *J. Mech. Des.*, vol. 123, no. 4, p. 525, 2001.
[26] G. Endo, H. Yamada, A. Yajima, M. Ogata, and S. Hirose, "A passive weight compensation mechanism with a non-circular pulley and a spring," in *Proc. IEEE Int. Conf. Robot. Autom.*, May 2010, pp. 3843–3848.
[27] H.-S. Kim and J.-B. Song, "Low-cost robot arm with 3-DOF counterbalance mechanism," in *Proc. IEEE Int. Conf. Robot. Autom.*, May 2013, pp. 4183–4188.
[28] M. Vermeulen and M. Wisse, "Intrinsically safe robot arm: Adjustable static balancing and low power actuation," *Int. J. Social Robot.*, vol. 2, no. 3, pp. 275–288, Sep. 2010.
[29] J. P. Whitney and J. K. Hodgins, "A passively safe and gravity-counterbalanced anthropomorphic robot arm," in *Proc. IEEE Int. Conf. Robot. Autom. (ICRA)*, May 2014, pp. 6168–6173.
[30] V. Van Der Wijk and J. L. Herder, "Force balancing of variable payload by active force-balanced reconfiguration of the mechanism," in *Proc. ASME/IFToMM Int. Conf. Reconfigurable Mech. Robots*, Jun. 2009, pp. 323–330.
[31] C. Baradat, V. Arakelian, S. Briot, and S. Guegan, "Design and prototyping of a new balancing mechanism for spatial parallel manipulators," *J. Mech. Des., Trans. ASME*, vol. 130, no. 7, pp. 0723051–07230513, 2008.
[32] V. Arakelian and S. Briot, *Mechanisms and Machine Science Balancing of Linkages and Robot Manipulators–Advanced Methods with Illustrative Examples*, vol. 27, M. Ceccarelli, Ed. Cham, Switzerland: Springer, 2015.
[33] Q. Wu, X. Wang, and F. Du, "Development and analysis of a gravity-balanced exoskeleton for active rehabilitation training of upper limb," *Proc. Inst. Mech. Eng., C, J. Mech. Eng. Sci.*, vol. 230, no. 20, pp. 3777–3790, Dec. 2016.
[34] H. Yu, I. S. Choi, K.-L. Han, J. Y. Choi, G. Chung, and J. Suh, "Development of a upper-limb exoskeleton robot for refractory construction," *Control Eng. Pract.*, vol. 72, pp. 104–113, Mar. 2018.
[35] M. A. Gull, S. Bai, and T. Bak, "A review on design of upper limb exoskeletons," *Robotics*, vol. 9, no. 1, p. 16, 2020.
[36] D. Ma and J. M. Hollerbach, "Identifying mass parameters for gravity compensation and automatic torque sensor calibration," in *Proc. IEEE Int. Conf. Robot. Autom.*, 1996, pp. 661–666.
[37] A. De Luca, B. Siciliano, and L. Zollo, "PD control with on-line gravity compensation for robots with elastic joints: Theory and experiments," *Automatica*, vol. 41, no. 10, pp. 1809–1819, Oct. 2005.
[38] A. Zavala-Rio and V. Santibanez, "A natural saturating extension of the PD-With-Desired-Gravity-Compensation control law for robot manipulators with bounded inputs," *IEEE Trans. Robot.*, vol. 23, no. 2, pp. 386–391, Apr. 2007.

[39] Y.-C. Liu and N. Chopra, "Gravity-Compensation-Driven position regulation for robotic systems under Input/Output delays," *IEEE Trans. Control Syst. Technol.*, vol. 22, no. 3, pp. 995–1005, May 2014.
[40] Z. Li, W. Zuo, and S. Li, "Zeroing dynamics method for motion control of industrial upper-limb exoskeleton system with minimal potential energy modulation," *Measurement*, vol. 163, Oct. 2020, Art. no. 107964.
[41] V. Arakelian, "Gravity compensation in robotics," *Adv. Robot.*, vol. 30, no. 2, pp. 79–96, Jan. 2016.
[42] A. T. Asbeck and A. Bolkhovitinov, "Method and mechanisms for providing gravity compensation to a human or robot arm," U.S. Patent App. 62 828 285, Apr. 2, 2019.
[43] J. L. Herder, N. Vrijlandt, T. Antonides, M. Cloosterman, and P. L. Mastenbroek, "Principle and design of a mobile arm support for people with muscular weakness," *J. Rehabil. Res. Develop.*, vol. 43, no. 5, p. 591, 2006.
[44] S. Schöneburg-Lehnert, *The Pantograph: A Historical Drawing Device for Math Teaching*. Cham, Switzerland: Springer, 2018, pp. 323–340.
[45] K. Fujikoshi, "Balancing apparatus for jointed robot," Jpn. Patent JP 51 122 254, Oct. 26, 1976.
[46] J. L. Herder and G. J. M. Tuijthof, "Two spatial gravity equilibrators," in *Proc. ASME Design Eng. Tech. Conf.*, 2000, pp. 1–9.
[47] (Apr. 2006). *Anthropometric Data*. NC State Univ. Ergonom. Center, p. 12. [Online]. Available: https://multisite.eos.ncsu.edu/www-ergocenter-ncsu-edu/wp-content/uploads/sites/18/2016/06/Anthropometric-Detailed-Data-Tables.pdf
[48] C. E. Clauser, J. T. McConville, and J. W. Young, *Weight, Volume, and Center of Mass of Segments of the Human Body (AMRL-TR-69-70)*. Yellow Springs, OH, USA: Wright Patterson Air Force Base, Aerospace Medical Research Laboratory, 1969, pp. 1–101.
[49] C. D. Fryar, Q. Gu, and C. L. Ogden, "Anthropometric reference data for children and adults; United States, 2007–2010," U.S. Department of Health and Human Services, Center for Disease Control and Prevent, Nat. Center Health Statist., Hyattsville, MD, USA, Tech. Rep., Oct. 2012, p. 7, 9, 13, 15.
[50] *Basic Gas Spring Theory*, 9th ed., Kaller, Tranås, Sweden, 2010. [Online]. Available: https://www.kaller.com/globalassets/support–download/files/basic-gas-spring-theory/basicgasspringtheoryed92010.pdf
[51] *Recommendations for Sensor Locations in Shoulder or Neck Muscles*. Seniam. [Online]. Available: http://seniam.org/deltoideusmedius.html
[52] V. Florimond, "Basics of surface electromyography applied to physical rehabilitation and biomechanics," *Thought Technol.*, pp. 14–16, Mar. 2010. [Online]. Available: https://www.thoughttechnology.com/pdf/manuals/MAR908-03%20SEMG%20applied%20to%20physical%20rehabilitation%20and%20biomechanics.pdf

JOSHUA HULL received the bachelor's degree in mechanical engineering from Virginia Tech, in 2019, where he is currently pursuing the master's degree in mechanical engineering. He has been a SMART Scholar with the U.S. Department of the Navy since 2018. His research interests include exoskeleton design, robotics, and controls engineering.

RANGER TURNER received the bachelor's degree in mechanical engineering from Virginia Tech, in 2019, where he is currently pursuing the master's degree with the Mechanical Engineering Program. His research interests include kinematic design, wearable robotics, and design workflows.

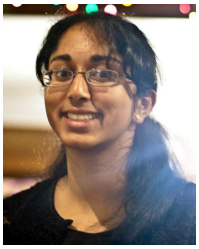

ATHULYA A. SIMON received the B.S. degree in biomedical engineering and the M.S. degree in robotics from Northwestern University, in 2014 and 2015, respectively. She is currently pursuing the Ph.D. degree in mechanical engineering with Virginia Tech. Her research interests include biomechanics, robotics, and human-assistance devices.

ALAN T. ASBECK received the Ph.D. degree in electrical engineering from Stanford University, in 2010. He is currently an Assistant Professor in mechanical engineering with Virginia Tech, Blacksburg, VA, USA. His current research interests include mechanism design, human-assistance devices, human sensing systems, and robotics.